

# Study of Simple MPPT Converter Topologies for Grid Integration of Photovoltaic Systems

Janis Zakis, *Tallinn University of Technology*,  
Dmitri Vinnikov, *Tallinn University of Technology*

**Abstract** – This paper presents a study of two simple MPPT converter topologies for grid integration of photovoltaic (PV) systems. A general description and a steady state analysis of the discussed converters are presented. Main operating modes of the converters are explained. Calculations of main circuit element parameters are provided.

Experimental setups of the MPPT converters with the power of 800 W were developed and verified by means of main operation waveforms. Also, experimental and theoretical boost properties of the studied topologies are compared.

Finally, the integration possibilities of the presented MPPT converters with a grid side inverter are discussed and verified by simulations.

**Keywords** – DC-DC power converters, photovoltaic systems, pulse inverters

## I. INTRODUCTION

Distributed generation systems that use renewable energy have great potential to increase the grid potential. Photovoltaic (PV) technology that provides renewable energy is the most popular distributed energy source with zero emissions.

PV cells have nonlinear  $U$ - $I$  characteristics. The output voltage and power change according to the temperature and irradiation.

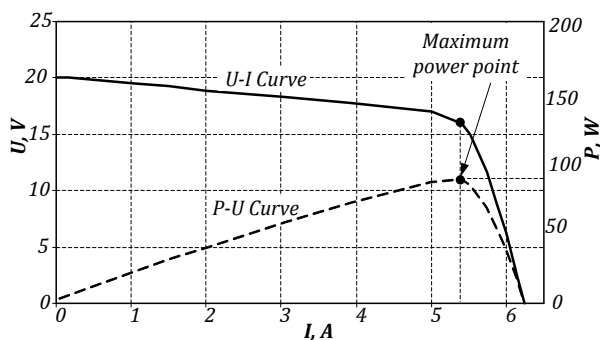


Fig. 1. Typical  $U$ - $I$  and  $P$ - $U$  characteristics of the PV stack.

Fig. 1 shows typical  $U$ - $I$  and  $P$ - $U$  characteristics of a PV stack. It can be seen that maximum power could be obtained only at one certain point – the maximal power point.

To keep the operation at the maximal power point independent of the temperature and irradiation, the maximal power point tracker (MPPT) converter should be used. Fig. 2 illustrates the general block diagram of a MPPT converter for AC or DC load applications in PV systems.

This paper presents a comparative evaluation of a classical boost converter (BC, Fig. 3a) and a quasi-Z-source converter (qZSC, Fig. 3b).

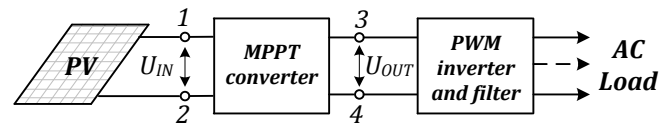


Fig. 2. General block diagram of a MPPT converter for a PV system.

## II. GENERAL DESCRIPTION OF STUDIED TOPOLOGIES

Simple MPPT converter topologies for grid integration of a PV system are shown in Fig. 3. The PWM inverter is replaced with an equivalent resistance  $R_E$ . Fig. 3a shows a BC which consists of an inductor  $L_1$ , a capacitor  $C_1$ , a diode  $D$ , and a switch  $S$  [1-3]. Fig. 3b shows a qZSC, which consists of two inductors  $L_1, L_2$  with equal inductance, two capacitors  $C_1, C_2$  with equal capacitance, a diode  $D$ , and a switch  $S$  across the DC-link [4].

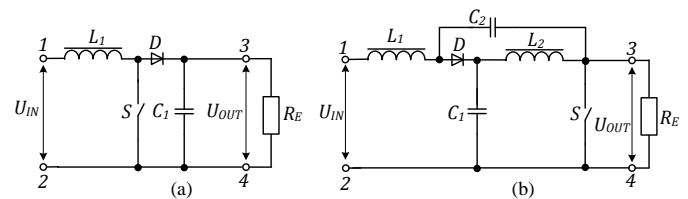


Fig. 3. Simple MPPT converter topologies: BC (a) and qZSC (b).

## III. STEADY-STATE ANALYSIS OF TOPOLOGIES OPERATED IN CONTINUOUS CONDUCTION MODE (CCM)

The steady state analysis for all the discussed converters is presented below. This operation comprises two main power conversion states: voltage boost (on-state of the switch  $S$ ) and power transfer (off-state of the switch  $S$ ). The operation period of the switch  $S$  consists of an on-state  $t_{ON}$  and an off-state  $t_{OFF}$ :

$$T = t_{ON} + t_{OFF} . \quad (1)$$

Eq. (1) could also be represented as

$$\frac{t_{ON}}{T} + \frac{t_{OFF}}{T} = D_{ON} + D_{OFF} = 1, \quad (2)$$

where  $D_{ON}, D_{OFF}$  are the duty cycles of the switch  $S$  on-state and off-state, correspondingly.

### A. Boost converter

Fig. 4 shows the equivalent circuits of a classical BC during the on- and off-state of the switch  $S$ . The switching state diagram of the BC is presented in Fig. 5.

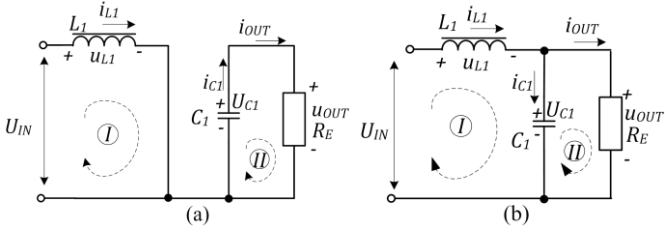


Fig. 4. Equivalent circuits of a BC: (a) switch  $S$  is on; (b) switch  $S$  is off.

From Fig. 4a, which represents the conditions when the switch  $S$  is on with the duration of  $t_{ON}$ , we obtain

$$u_{L1} = U_{IN}; i_{C1} = -\frac{U_{C1}}{R_E}. \quad (3)$$

From Fig. 4b, which represents the conditions when the switch  $S$  is opened with the duration of  $(T - t_{ON})$ , we obtain

$$u_{L1} = U_{IN} - U_{C1}. \quad (4)$$

At the steady state the average voltage of the inductor over one switching period is zero:

$$U_{L1} \cdot (t_{ON}) + U_{L1}(t_{OFF}) = 0. \quad (5)$$

Thus, from Eqs. (3) and (5) we obtain

$$U_{L1} = \bar{U}_{L1} = \frac{U_{IN} \cdot (t_{ON}) + (U_{IN} - U_{C1}) \cdot (1 - t_{ON})}{T} = 0. \quad (6)$$

Accordingly,

$$U_{C1} = \frac{U_{IN}}{1 - t_{ON}}. \quad (7)$$

The output voltage is

$$u_{OUT} = U_{C1} = \frac{1}{1 - D_{ON}} \cdot U_{IN} = B \cdot U_{IN}, \quad (8)$$

where  $B$  is the boost factor of the BC

$$B = \frac{1}{1 - D_{ON}}. \quad (9)$$

The inductor in the converter will limit the current ripple through the switch  $S$  during its on-state. Choosing an acceptable peak to peak current ripple  $r_{C,(%)}$  the inductance  $L_1$  of the inductor can be calculated as

$$L_1 = \frac{U_{L1} dt}{di_{L1}}. \quad (10)$$

where

$$U_{L1} = U_{IN}; dt = D_{ON} \cdot T = \frac{D_{ON}}{f}; di_{L1} = \frac{P}{U_{IN}} \cdot r_{C,(%)}, \quad (11)$$

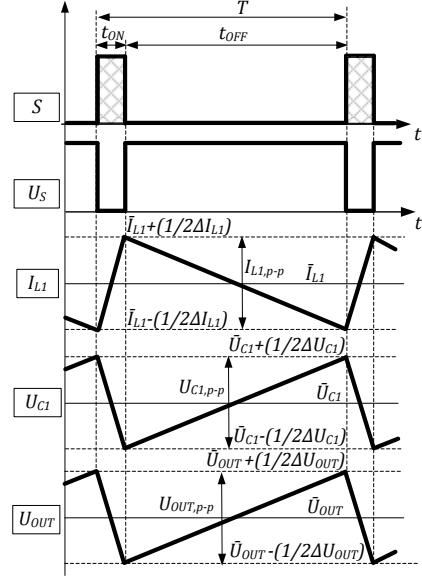


Fig. 5. Operation principle of the BC.

Using (10) and (11), the inductance  $L_1$  of the inductor can be calculated as

$$L_1 = \frac{U_{IN}^2 \cdot D_{ON}}{f \cdot P \cdot r_{C,(%)}} \quad (12)$$

where  $P$  is the power rating of the converter,  $U_{IN}$  is the input voltage,  $f$  is the operation frequency of the converter, and  $r_{C,(%)}$  is the desired peak to peak current ripple through the inductor ( $I_{p-p}/\bar{I}$ ).

Using the system power rating  $P$  we can obtain the average current of the inductor  $L_1$ :

$$\bar{I}_{L1} = \bar{I}_{IN} = \frac{P}{U_{IN}}. \quad (13)$$

The operating voltages and average currents of the BC during the switch  $S$  on-state and an off-state are shown in Table I.

The main purpose of the capacitor  $C_1$  is to absorb the current ripple and limit the voltage ripple across the load resistance  $R_E$ . The voltage ripple across the capacitor can be roughly calculated by

$$\Delta U_{C1} = \frac{\bar{I}_L \cdot \Delta t}{C_1}, \quad (14)$$

where  $\bar{I}_{L1}$  is the average current through the inductor,  $C_1$  is the capacitance and  $\Delta t$  is the time interval of the on-state of the switch. The capacitance needed to limit the peak to peak output voltage ripple by  $r_{V,(%)}$  could be calculated as

$$C_1 = \frac{P \cdot D_{ON} \cdot (1 - D_{ON})^2}{U_{IN}^2 \cdot f \cdot r_{V,(%)}} \quad (15)$$

where  $P$  is the power rating of the converter,  $U_{IN}$  is the input voltage,  $D_{ON}$  is the duty cycle of the on-state of the switch,  $f$  is the operation frequency of the switch  $S$ , and  $r_{V,(%)}$  is the

desired peak to peak voltage ripple across the capacitor ( $U_{p-p}/\bar{U}$ ).

TABLE I  
OPERATING VOLTAGES AND CURRENTS OF THE BC

Time interval	$t_{ON}$	$t_{OFF}$
Inductor $L_1$ voltage ( $u_{L1}$ )	$U_{IN}$	$\frac{U_{IN} \cdot D_{ON}}{1 - D_{ON}}$
Diode $D$ voltage ( $u_D$ )	$-\frac{U_{IN}}{1 - D_{ON}}$	0
Capacitor $C_1$ voltage ( $U_{C1}$ )	$\frac{U_{IN}}{1 - D_{ON}}$	
Input current ( $\bar{I}_{IN}$ )	$\frac{P}{U_{IN}}$	
Inductor current ( $\bar{I}_{L1}$ )	$\frac{P}{U_{IN}}$	
Capacitor current ( $\bar{I}_{C1}$ )	$I_D \cdot I_{OUT}$	
Diode current ( $i_D$ )	0	$I_C + I_{OUT}$
Output current ( $\bar{I}_{OUT}$ )	$\frac{P \cdot (1 - D_{ON})}{U_{IN}}$	

### B. qZS-Converter

Fig. 6 illustrates the equivalent circuits of the qZSC in both on-state and off-state of the switch  $S$ . The switching state diagram of the qZSC is presented in Fig. 7.

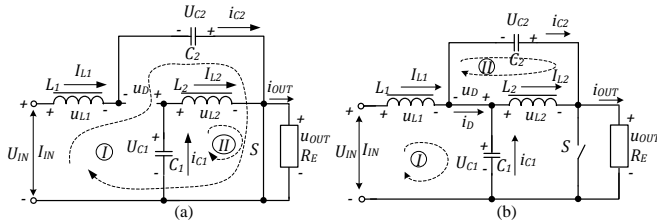


Fig. 6. Equivalent circuits of the qZSC during the on-state (a) and off-state (b).

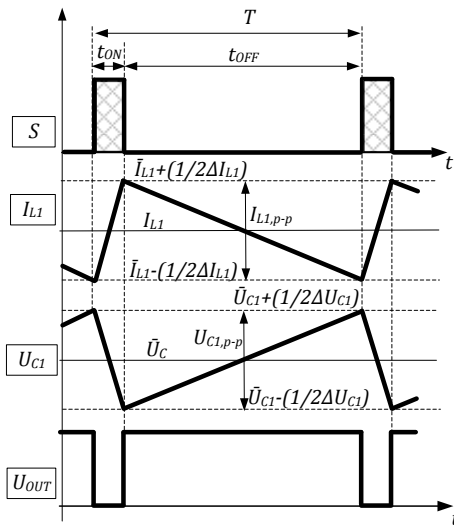


Fig. 7. Operation principle of the qZSC.

From Fig. 6a, which represents the on-state of the switch  $S$  with duration  $t_{ON}$ , we obtain

$$u_{L1} = U_{C2} + U_{IN}; \quad u_{L2} = U_{C1}. \quad (16)$$

$$u_{DC} = 0; \quad u_D = U_{C1} + U_{C2}. \quad (17)$$

From Fig. 6b, which represents the off-state of the switch  $S$  with the duration of  $(T - t_{ON})$ , we obtain

$$u_{L1} = U_{IN} - U_{C1}; \quad u_{L2} = -U_{C2}. \quad (18)$$

$$u_{DC} = U_{C1} - u_{L2} = U_{C1} + U_{C2}; \quad u_D = 0. \quad (19)$$

At the steady state the average voltage of the inductor over one switching period is zero. Thus, from Eqs. (16) and (18) we obtain

$$\begin{cases} U_{L1} = u_{L1} = \frac{t_{ON} \cdot (U_{C2} + U_{IN}) + (T - t_{ON}) \cdot (U_{IN} - U_{C1})}{T} = 0 \\ U_{L2} = u_{L2} = \frac{t_{ON} \cdot (U_{C1}) + (T - t_{ON}) \cdot (-U_{C2})}{T} = 0 \end{cases}. \quad (20)$$

Accordingly,

$$U_{C1} = \frac{1 - D_{ON}}{1 - 2 \cdot D_{ON}} \cdot U_{IN} \quad \text{and} \quad U_{C2} = \frac{D_{ON}}{1 - 2 \cdot D_{ON}} \cdot U_{IN}. \quad (21)$$

The output voltage is

$$u_{OUT} = U_{C1} + U_{C2} = \frac{1}{1 - 2D_{ON}} \cdot U_{IN} = B \cdot U_{IN}, \quad (22)$$

where  $B$  is the boost factor of the qZSC:

$$B = \frac{1}{1 - 2 \cdot D_{ON}}. \quad (23)$$

Using the system power rating  $P$  we can obtain the average current of the inductors  $L_1$  and  $L_2$ :

$$\bar{I}_{L1} = \bar{I}_{L2} = \bar{I}_{IN} = \frac{P}{U_{IN}}, \quad (24)$$

where  $U_{IN}$  and  $I_{IN}$  are the input voltage and current of the converter. To obtain the necessary currents of the qZSC we can use Kirchoff's current law:

$$\bar{I}_{C1} = \bar{I}_{C2} = \bar{I}_{OUT} - \bar{I}_{L1}. \quad (25)$$

$$\bar{I}_{D1} = 2\bar{I}_{L1} - \bar{I}_{OUT}. \quad (26)$$

The operating voltages and currents of the qZSC during on- and off-states are shown in Table II. The main purpose of capacitors  $C_1$  and  $C_2$  is to absorb the current ripple and limit the voltage ripple across the switch  $S$ . The capacitor voltage ripple can be roughly calculated by (14).

TABLE II  
OPERATING VOLTAGES AND CURRENTS OF THE qZSC

Time interval	$t_{ON}$	$t_{OFF}$
Inductor voltage ( $u_{L1}=u_{L2}$ )	$-\frac{D_{ON}}{1-2 \cdot D_{ON}} \cdot U_{IN}$	$-\frac{1-D_{ON}}{1-2 \cdot D_{ON}} \cdot U_{IN}$
Output voltage ( $u_{OUT}$ )	$\frac{1}{1-2 \cdot D_{ON}} \cdot U_{IN}$	0
Output current ( $\bar{I}_{OUT}$ )	$\frac{P \cdot (1-2 \cdot D_{ON})}{U_{IN}}$	$\frac{2 \cdot P}{U_{IN}} \cdot D_{ON}$
Diode $D_1$ voltage ( $u_D$ )	0	$\frac{1}{1-2 \cdot D_{ON}} \cdot U_{IN}$
Capacitor $C_1$ voltage ( $U_{C1}$ )	$\frac{1-D_{ON}}{1-2 \cdot D_{ON}} \cdot U_{IN}$	
Capacitor $C_2$ voltage ( $U_{C2}$ )	$\frac{D_{ON}}{1-2 \cdot D_{ON}} \cdot U_{IN}$	
Input current ( $\bar{I}_{IN}$ )	$\frac{P}{U_{IN}}$	
Inductor current ( $\bar{I}_{L1}=\bar{I}_{L2}$ )	$\frac{P}{U_{IN}}$	
Capacitor current ( $\bar{I}_{C1}=\bar{I}_{C2}$ )	$\bar{I}_{DC} - \bar{I}_{L1}$	
Diode current ( $\bar{I}_D$ )	$2 \cdot \bar{I}_{L1} - \bar{I}_{DC}$	

During the off-state, both capacitors of the qZSC are in series (Fig. 6b). Assuming that the capacitance should be the same for each capacitor, the capacitance needed to limit the peak to peak DC-link voltage ripple by  $r_{V,(%)}$  could be calculated as

$$C = \frac{2 \cdot P \cdot D_{ON} \cdot (1-2D_{ON})}{U_{IN}^2 \cdot (1-D_{ON}) \cdot f \cdot r_{V,(%)}} \quad (27)$$

where  $P$  is the power rating of the converter,  $U_{IN}$  is the input voltage,  $D_{ON}$  is the duty cycle of on-state,  $f$  is the operation frequency of the switch  $S$ , and  $r_{V,(%)}$  is the desired peak to peak voltage ripple across the load  $R_E$  ( $U_{pp}/\bar{U}$ ).

The inductor in the qZSC network will limit the current ripple through the switch  $S$  during the on-state. Choosing an acceptable peak to peak current ripple  $r_{C,(%)}$  the inductance can be calculated by

$$L = \frac{U_{IN}^2 \cdot (1-D_{ON}) \cdot D_{ON}}{(1-2D_{ON}) \cdot f \cdot P \cdot r_{C,(%)}} \quad (28)$$

where  $P$  is the power rating of the converter,  $U_{IN}$  is the input voltage,  $U_{C1}$  is the capacitor's  $C_1$  voltage,  $D_{ON}$  is the duty cycle of on-states,  $f$  is the operation frequency of the switch  $S$ , and  $r_{C,(%)}$  is the desired peak to peak current ripple through the inductor ( $I_{p-p}/\bar{I}$ ).

#### IV. EXPERIMENTAL VERIFICATION

To verify the theory discussed above three experimental setups with the rated power of 800 W were developed and tested in the same conditions. It was stated that the input voltage ( $U_{IN}=40$  V) should be boosted two times ( $U_{OUT}=80$  V).

To obtain the desired twofold boost the on-state duty cycles of the switch  $S$  were set to 0.5 for the BC and 0.25 for the qZSC. As Table III shows, the capacitors and inductors implemented in both topologies have similar values.

TABLE III  
COMPONENT TYPES AND VALUES USED IN EXPERIMENTS

Component	BC	qZSC
Inductor $L_1$	110 $\mu$ H	
Inductor $L_2$	---	110 $\mu$ H
Capacitor $C_1$	120 $\mu$ F	
Capacitor $C_2$	---	120 $\mu$ F
Diode $D$	STTH200L06TV1	
Switch $S$	SKM50GB123D	

Fig. 8 presents the main operating waveforms of the discussed converters. These are input voltage ( $U_{IN}$ ), input current ( $I_{L1}$ ), output voltage ( $U_{OUT}$ ), and output current ( $I_{OUT}$ ). It is obvious that both converters can step up the input voltage two times. Fig. 8 shows that BC features the DC output voltage while the qZSC has the square wave output voltage waveform. The output current and voltage ripple of the BC is almost negligible. However, the qZSC has the input current ripple reduced by 10% as compared to BC, which is especially topical in applications with renewable energy sources. Finally, for the same component types and values the qZSC has smaller ringing in the input voltage profile (which is mostly caused by switching transients), and, consequently, reduced stress of the solar panel and smaller EMI impact.

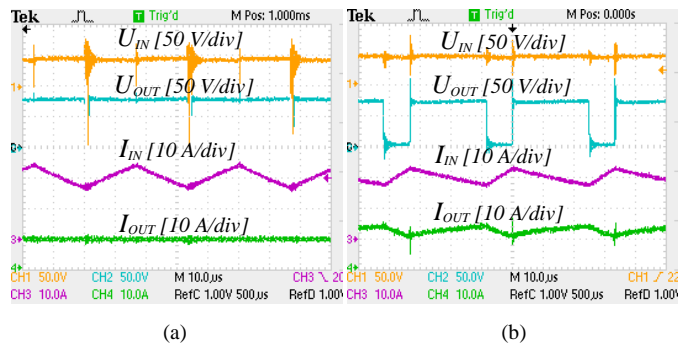


Fig. 8. Main operation waveforms of the BC (a) and the qZSC (b) MPPTs: input voltage ( $U_{IN}$ ) and current ( $I_{IN}$ ), output voltage ( $U_{OUT}$ ) and current ( $I_{OUT}$ ).

In the second experiment the voltage boost properties were examined for each converter and compared to those theoretically predicted. Relation between the converter output voltage  $U_{OUT}$  and the switch on-state duty cycle  $D_{ON}$  is shown in Fig. 9. It was stated that the twofold voltage boost can be achieved with both the BC and the qZSC, though the qZSC requires twice smaller on-state duty cycle  $D_{ON}$  of the switch  $S$ . It can be explained by the number of energy storage elements that is doubled. Fig. 9 also shows that at a larger  $D_{ON}$  value the experimental curve becomes lower than the theoretical curve. This fact can be explained by the voltage drop on the circuit elements, mostly in semiconductors.

Fig. 10 shows the inductance  $L$  as a function of the boost factor  $B$  for the discussed converters for the current ripple of

20%. It can be seen that for the same boost factor  $B$  the inductance of the inductor must be about 40% larger for the BC as compared to the qZSC. In contrast to the BC, the qZSC requires one additional inductor, which could impose an additional space and weight requirements. However, utilizing the coupled inductors with common mode coupling as described in [5], the twice reduced inductance value of each inductor could be assumed for the same input current ripple.

Fig. 11 shows the capacitance  $C$  as a function of the boost factor  $B$  for the discussed converters. The capacitance of capacitors  $C_1$  and  $C_2$  of the qZSC for the twofold boost and assumed 5% ripple should be two times higher than for BC and in the case of twofold boost, the difference is even.

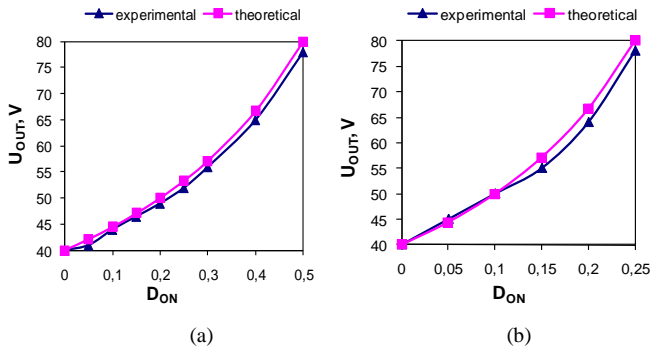


Fig. 9. Experimental and theoretical boost properties of the BC (a) and the qZSC (b).

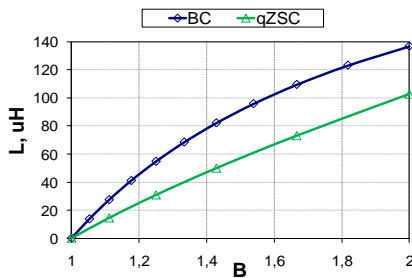


Fig. 10. Inductance of inductors of the BC and the qZSC as a function of the boost factor.

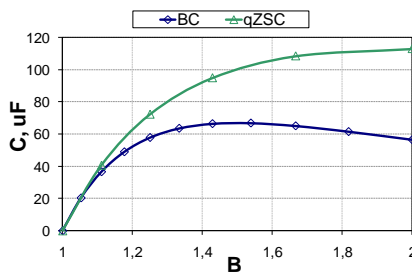


Fig. 11. Capacitance of capacitors of the BC and the qZSC as a function of the boost factor.

## V. INTEGRATION POSSIBILITIES WITH A GRID SIDE INVERTER

In most cases the connection of PV with a grid is realized by the topology presented in Fig. 2. Since the DC voltage generated by a PV stack varies widely, a MPPT converter is essential to generate a regulated voltage. A DC-AC inverter is essential to provide useful AC power at 50 Hz frequency. An

output LC filter connected to the inverter filters the switching frequency harmonics and generates a high quality sinusoidal AC waveform suitable for the dedicated loads.

This section discusses the possibilities of integration of discussed MPPT converters with the grid side inverter in order to reduce the number of switching elements, simplify the control circuits and increase the power density.

### A. Boost converter

The BC cannot be integrated to the grid side inverter and could be only implemented as an auxiliary converter with separate control (Fig. 12). The presented cascaded arrangement of the BC and the grid side inverter increases both the complexity of the power circuit and the controller and the cost and space requirements. Moreover, the increased number of power switches results in a lower efficiency.

The full-bridge inverter with an LC filter inverts the intermediate DC link voltage into AC voltage. The unipolar modulation technique is used for the inverter control to reduce the switching losses and output filter size [6]. The sine wave signal and the inverter sine wave signal are compared there with a bipolar triangle signal in order to obtain gate signals for transistors  $T_1$  and  $T_3$ . The inversed signals drive the opposite transistors  $T_2$  and  $T_4$ .

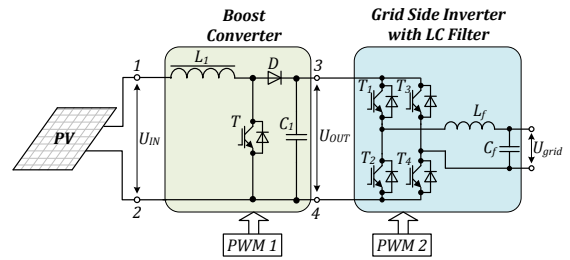


Fig. 12. BC based interface converter for grid integration of PV systems.

If the small voltage drop and phase shift in the LC filter are neglected, then the output voltage of the inverter is

$$u_{grid} = U_{IN} \cdot \frac{M_i}{1 - D_{ON}} \cdot \sin(\omega t), \quad (29)$$

where  $M_i$  is the modulation index of the inverter. Fig. 13 shows the simulation results of the topology presented in Fig. 12. It was assumed that the output voltage of the PV stack is 160 VDC. The boost converter operating with the duty cycle of 0.5 is stepping up the input voltage to the level of 320 VDC, which is essential to generate the grid side AC voltage with an rms value of 230 V.

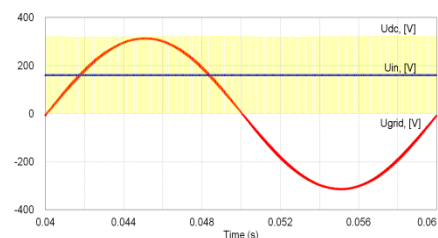


Fig. 13. Simulation results of the BC based interface converter.

### B. qZS-Converter

A marked advantage of the qZSC is that it could be fully integrated with the grid side inverter (Fig. 14). The topology presented is also referred to as a quasi-Z-source inverter (qZSI, [7, 8]), consisting of the unique LC and diode network (qZS-network) connected to the inverter bridge. The function of the switch  $S$  (Fig. 3b) could be fully replaced by the special switching state of the inverter – the shoot-through state, when both switches of one inverter leg are simultaneously switched on. The qZS-network will effectively protect the circuit from damage when the shoot-through occurs and also could boost the input voltage to a higher level simply by the variation of the shoot-through duty cycle. Neglecting losses in components the output voltage of the inverter could be estimated as

$$u_{grid} = U_{IN} \cdot B \cdot M_i \cdot \sin(\omega t) = U_{IN} \cdot \frac{1 - D_S}{1 - 2D_S} \cdot \sin(\omega t), \quad (30)$$

where  $D_S$  is the shoot-through duty cycle.

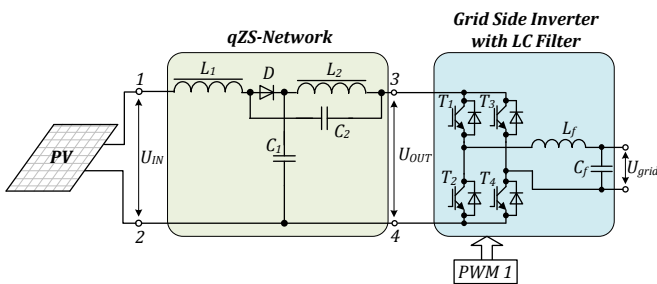


Fig. 14. qZSC based interface converter for grid integration of PV systems.

Fig. 15 shows the simulation results of the qZSC based interface converter for grid integration of PV systems. It was assumed that the output voltage of the PV stack is 160 VDC. In order to obtain the grid side AC voltage with an rms value of 230 V the shoot-through duty cycle was set to 0.33. The intermediate DC-link voltage  $U_{DC}$  was stepped up to the level of 490 V, which is essential to generate the sinusoidal voltage at the given modulation factor ( $M_i=1-D_S=0.66$ ) and with the required amplitude of 320 V.

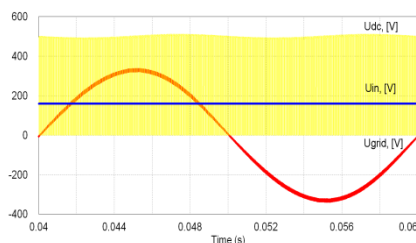


Fig. 15. Simulation results of the qZSC based interface converter.

## VI. CONCLUSIONS

This paper presents a comparative study of simple MPPT converter topologies for the PV system integration with a grid. The MPPT converter topologies were described in detail and an analysis of operation states and calculations of voltages, currents and circuit parameters were presented. The experimental results showed that the discussed converters

have necessary voltage boost properties and can be used for the MPPT function.

Finally, the integration possibilities of the presented MPPT converters with a grid side inverter were discussed and verified by simulations. The simulation results show that the discussed converters which are coupled with a grid side inverter can boost input DC voltage and can ensure sinusoidal voltage with an rms value of 230V at the AC load or grid.

### ACKNOWLEDGEMENTS

This research work was supported by the Estonian Ministry of Education and Research (Project SF0140016s11), Estonian Science Foundation (Grant ETF8538) and European Social Fund's Researcher Mobility Program "Mobilitas" (MJD42).

### REFERENCES

- [1] N. Mohan, T. M. Undeland, and W. P. Robbins, Power Electronics. Converters, Applications and Design: Wiley, 2003, pp. 161-200.
- [2] Shanthi, T.; Ammasai Gounden, N., "Power electronic interface for grid-connected PV array using boost converter and line-commutated inverter with MPPT," International Conference on Intelligent and Advanced Systems ICIAS 2007, pp.882-886, 2007.
- [3] Ribeiro, H.; Pinto, A.; Borges, B., "Single-stage DC-AC converter for photovoltaic systems," Energy Conversion Congress and Exposition (ECCE), 2010, pp. 604-610, 2010.
- [4] R. Strzelecki, D. Vinnikov, "Models of the qZ-Converters," *Przegląd Elektrotechniczny*, vol. 86 (6), 2010, pp. 80-84.
- [5] Zakis, J.; Vinnikov, D.; Bisenieks, L. "Some Design Considerations for Coupled Inductors for Integrated Buck-Boost Converters", III International Conference on Power Engineering, Energy and Electrical Drives POWERENG 2011, pp. 1-6, 2011.
- [6] Bisenieks, L.; Vinnikov, D.; Zakis, J. "Analysis of Operating Modes of the Novel Isolated Interface Converter for PMSG Based Wind Turbines", III International Conference on Power Engineering, Energy and Electrical Drives POWERENG 2011, pp. 1-8, 2011.
- [7] Anderson, J.; Peng, F.Z., "Four quasi-Z-Source inverters," IEEE Power Electronics Specialists Conference PESC 2008, pp. 2743-2749, 2008.
- [8] Yuan Li; Anderson, J.; Peng, F.Z.; Dichen Liu, "Quasi-Z-Source Inverter for Photovoltaic Power Generation Systems," presented at 24th Applied Power Electronics Conference and Exposition, APEC 2009.

**Janis Zakis** (M'10) received B.Sc., M.Sc. and Dr.Sc.ing. in electrical engineering from Riga Technical University, Riga, Latvia, in 2002, 2004 and 2008, respectively.

He is presently a Senior Researcher in the Department of Electrical Drives and Power Electronics, Tallinn University of Technology.

He has over 20 publications and is the holder of one Utility Model in power converter design. His research interests include flexible ac transmission systems (FACTS), simulation of power systems, switching mode power converters, applied design of power converters and energy storage systems.



**Dmitri Vinnikov** (M'07) received Dipl.Eng., M.Sc. and Dr.Sc.techn. in electrical engineering from Tallinn University of Technology, Tallinn, Estonia, in 1999, 2001 and 2005, respectively.

He is presently a Senior Researcher in the Department of Electrical Drives and Power Electronics, Tallinn University of Technology. He has authored more than 100 published papers on power converters design and development. His research interests include switchmode power converters, modeling and simulation of power systems, applied design of

power converters and control systems and application and development of energy storage systems.

